The Journal of Experimental Biology 210, 2368-2382
Published by The Company of Biologists 2007
doi:10.1242/jeb.005686

Three-dimensional kinematics of hummingbird flight

Bret W. Tobalske[1,*], Douglas R. Warrick[2], Christopher J. Clark[3], Donald R. Powers[4], Tyson L. Hedrick[5], Gabriel A. Hyder[1] and Andrew A. Biewener[6]

[1]Department of Biology, University of Portland, 5000 N. Willamette Boulevard, Portland, OR 97203, USA, [2]Department of Zoology, Oregon State University, 2002 Cordley Hall, Corvallis, OR 97331, USA, [3]Department of Integrative Biology, University of California, Berkeley, 3060 Valley Life Sciences Building # 3140, Berkeley, CA 94720, USA, [4]Biology Department, George Fox University, 414 N. Meridian Street, Newberg, OR 97132, USA, [5]Department of Biology, University of North Carolina, Chapel Hill, NC 27599 USA and [6]Concord Field Station, Department of Organismic and Evolutionary Biology, Harvard University, Old Causeway Road, Bedford, MA 01730, USA

*Author for correspondence (e-mail: tobalske@up.edu)

Accepted 24 April 2007

Summary

Hummingbirds are specialized for hovering flight, and substantial research has explored this behavior. Forward flight is also important to hummingbirds, but the manner in which they perform forward flight is not well documented. Previous research suggests that hummingbirds increase flight velocity by simultaneously tilting their body angle and stroke-plane angle of the wings, without varying wingbeat frequency and upstroke: downstroke span ratio. We hypothesized that other wing kinematics besides stroke-plane angle would vary in hummingbirds. To test this, we used synchronized high-speed (500 Hz) video cameras and measured the three-dimensional wing and body kinematics of rufous hummingbirds (*Selasphorus rufus*, 3 g, *N*=5) as they flew at velocities of 0–12 m s^{-1} in a wind tunnel. Consistent with earlier research, the angles of the body and the stroke plane changed with velocity, and the effect of velocity on wingbeat frequency was not significant. However, hummingbirds significantly altered other wing kinematics including chord angle, angle of attack, anatomical stroke-plane angle relative to their body, percent of wingbeat in downstroke, wingbeat amplitude, angular velocity of the wing, wingspan at mid-downstroke, and span ratio of the wingtips and wrists. This variation in bird-centered kinematics led to significant effects of flight velocity on the angle of attack of the wing and the area and angles of the global stroke planes during downstroke and upstroke. We provide new evidence that the paths of the wingtips and wrists change gradually but consistently with velocity, as in other bird species that possess pointed wings. Although hummingbirds flex their wings slightly at the wrist during upstroke, their average wingtip–span ratio of 93% revealed that they have kinematically 'rigid' wings compared with other avian species.

Key words: Rufous hummingbird, *Selasphorus rufus*, kinematics, flight.

Introduction

Hummingbirds (Trochilidae) are best known for their sustained hovering abilities, but they also regularly use forward flight. Both types of flight are central to the ecology of hummingbirds. While they routinely hover during foraging and displaying (Greenewalt, 1960a; Wells, 1993; Stiles, 1982; Altshuler and Dudley, 2002), they must also fly between foraging locations, at which time their velocities range from 5 to 11 m s^{-1} (Gill, 1985). Laboratory tests have shown that they are capable of even greater forward velocities, exceeding 13 m s^{-1} (Greenewalt, 1960a; Chai and Dudley, 1999; Chai et al., 1999). Some species migrate long distances; the total migration distance for the rufous hummingbird (*Selasphorus rufus*) may exceed 6000 km, and the ruby-throated hummingbird *Archilocus colubris* migrates, non-stop, over the Gulf of Mexico (Calder, 1993; Robinson et al., 1996).

Many aspects of hovering have been studied in hummingbirds, including kinematics (Stolpe and Zimmer, 1939; Greenewalt, 1960a; Greenewalt, 1960b; Weis-Fogh, 1973), physiology (Weis-Fogh, 1972; Epting, 1980; Bartholomew and Lighton, 1986; Wells, 1993; Chai and Dudley, 1996) and aerodynamics (Warrick et al., 2005). Indeed, hummingbirds have emerged as a model assemblage for investigating maximal power capacity during hovering and climbing flight through the use of hypoxic, hypobaric and load-lifting protocols (Chai and Dudley, 1995; Chai and Dudley, 1999; Chai and Millard, 1997; Chai et al., 1999; Altshuler and Dudley, 2002; Altshuler et al., 2004). A prominent feature of

wing motion during hovering in hummingbirds is pronounced supination about the long axis of the wing during upstroke, which is associated with a 'figure-8' path of the wingtip in lateral projection (Stolpe and Zimmer, 1939; Greenewalt, 1960a). It was formerly thought that hovering downstroke and upstroke were kinematically and aerodynamically symmetrical, with each supporting body weight equally over each half of the wingbeat cycle (Stolpe and Zimmer, 1939; Greenewalt, 1960a; Greenewalt, 1960b; Weis-Fogh, 1972; Weis-Fogh, 1973).

This assumption of symmetry between half strokes needs to be revisited with new data, particularly because the aerodynamics of hovering are likely to be unsteady and, therefore, challenging to predict from kinematics (Spedding, 1993, Dickinson et al., 1999). Kinematics of similarly sized hovering hawkmoths *Manduca sexta* (Willmott and Ellington, 1997b) lead to an estimate that the upstroke produces more lift than downstroke, while flow visualization about a dynamically scaled model indicates the downstroke produces more lift due, in part, to leading-edge vorticity (Van den Berg and Ellington, 1997; Willmott et al., 1997). For the hovering hummingbird, the camber of the wing is different during the two halves of the wingbeat, and wake measurements indicate the majority (75%) of the weight support is provided by downstroke, while upstroke supports 25% (Warrick et al., 2005).

In contrast with the wealth of data available on hovering performance in hummingbirds, relatively little is known about how hummingbirds accomplish forward flight (Altshuler and Dudley, 2002). Greenewalt (Greenewalt, 1960a) presents lateral-view illustrations of wing paths and body postures of ruby-throated hummingbirds flying at 0, 4 and 13 m s^{-1} along with brief descriptions of wing kinematics at these velocities that include wingbeat frequency, downstroke fraction of the wingbeat cycle, and advance ratio. Data on long-axis rotation of the wing (pronation or supination) are lacking. Recent studies report maximum forward-flight velocities but not the associated wing kinematics (Chai et al., 1999; Chai and Dudley, 1999). From Greenwalt's description (Greenwalt, 1960a), it would appear that hummingbirds vary flight velocity primarily by changing the angle of their body relative to horizontal (β), thereby effecting a change in stroke-plane angle, as well as potentially varying their wingbeat amplitude (ϕ), which is known to vary according to power demands during hovering (Altshuler and Dudley, 2002; Altshuler and Dudley, 2003). Lateral-view figures representing the path of the wingtip hint (assuming the birds are drawn to the same scale) that ϕ may be less during forward flight at intermediate velocity compared with during hovering or fast flight (Greenewalt, 1960a). Paths of the wing in lateral projection also change from a figure-8 shape to an ellipse as hummingbirds change from hovering to forward flight (Greenewalt, 1960a).

No significant variation is reported for wingbeat frequency (f), the relative duration of the downstroke, or wing length (l) within the wingbeat cycle (Greenewalt, 1960a; Greenewalt, 1960b). Constant l would mean that upstroke:downstroke span ratio would be 100%, at all flight velocities, and this has important implications for the aerodynamics of flapping flight. Most birds in forward flight decrease their span ratio using wing flexion during upstroke to avoid producing negative thrust that is of equal magnitude to the positive thrust that they produced during downstroke (Rayner, 1986; Rayner, 1988; Tobalske, 2000). Assuming hummingbirds do not flex their wings and reduce their span during upstroke, they must change other parameters such as angular velocity or angle of attack of the wing to reduce upstroke circulation and lift so that they can sustain forward flight. Variation in circulation about the wings would lead to the shedding of a ladder-like wake structure with 'rungs' of cross-stream starting and stopping vortices into the wake and inflation of induced drag relative to a constant-circulation wake (Rayner, 1986). Recent kinematic evidence suggests that angle of attack and circulation varies throughout the wingbeat cycle in cockatiels *Nymphicus hollandicus* (Hedrick et al., 2002), and studies of wake structure reveal that regular shedding of cross-stream vortices is a characteristic of fast flight in passerines (Spedding et al., 2003; Hedenström et al., 2006).

Advances in technology since Greenewalt's pioneering research (Greenewalt, 1960a; Greenewalt, 1960b) allow us to explore more fully how kinematics of the wings and body of hummingbirds might vary with flight velocity. Given that, even during hovering, hummingbird flight is more consistent with the flight of other birds than previously believed (Warrick et al., 2005), we predicted that hummingbirds would vary aspects of their wing kinematics in a manner similar to other bird species (Brown, 1953; Brown, 1963; Tobalske and Dial, 1996; Tobalske, 2000; Park et al., 2001; Hedrick et al., 2002; Tobalske et al., 2003a; Tobalske et al., 2003b; Rosén et al., 2004).

Materials and methods

Birds and wind tunnel

Five female rufous hummingbirds *Selasphorus rufus* Gmelen 1788 (body mass 3.4 g, Table 1) were captured from the wild under permits from the US Fish and Wildlife Service and Oregon Department of Fish and Wildlife. All housing and experimental protocols were approved by the University of Portland Institutional Animal Care and Use Committee. During captivity, birds were housed in 1 m×1 m×1 m flight cages with *ad libitum* access to food and water in the form of Nektar-Plus (NEKTON®; Günter Enderle, Pforzheim, Baden-Württemberg, Germany) or a 20% sucrose solution.

We measured the morphology of the birds with their wings spread as in mid-downstroke using standard techniques (Tobalske et al., 1999) (Table 1). Linear measurements (mm) were obtained using digital calipers and metric rulers. Areas (mm^2) were measured from digital images using a known pixel-to-metric conversion. Average wing chord (mm) was calculated as wing area divided by wingspan. Aspect ratio (dimensionless) was calculated as wingspan divided by wing chord. Disc loading (N m^{-2}) was computed as body weight divided by disc area (S_d). For this instance, we assumed $S_d=\pi(b/2)^2$, with b=wing span. Wing loading (N m^{-2}) was

Table 1. *Morphological data for the rufous hummingbird (Selasphorus rufus)*

Variable	Value
Body mass (g)	3.4±0.1
Single wing length (mm)	47±1
Wing span, *b* (mm)	109±2
Average wing chord, *c* (mm)	12±1
Aspect ratio	9±1
Single wing area (mm^2)	558±18
Combined area of both wings and body (mm^2)	1346±108
Wing loading ($N\ m^{-2}$)	25±3
Disc loading ($N\ m^{-2}$)	3.6±0.2

Values are mean ± s.d. (*N*=5).

computed using body weight (N) divided by combined wing area, including the projected surface area of the body between the wings.

Our wind tunnel was designed for studies of avian flight at the University of Portland (Tobalske et al., 2005a). The tunnel is an open circuit with a closed jet, featuring a 6:1 contraction ratio and a total length of 6.1 m. The working section in which the bird flies is square in cross-section, 60 cm×60 cm×85 cm inner diameter at the inlet, with clear lexan walls, 6-mm thick, used to provide views inside the working section. The flight chamber increases to a 61.5 cm×61.5 cm outlet to accommodate boundary-layer thickening. Air is drawn through the tunnel using 7.5 kW (10 horsepower) direct current motor and a 0.75 m diameter fan assembly (AFS-75 Series, SMJ Incorporated, Grand Junction, CO, USA). Velocity (*V*) is selected as equivalent air velocity rather than true air velocity (Pennycuick et al., 1997; Hedrick et al., 2002). With a protective screen of vertical wires in place at the inlet of the working section, maximum deviations in velocity within a cross section are <10% of the mean, the boundary layer is <1 cm thick, and turbulence is 1.2% (Tobalske et al., 2005a).

Birds were acclimated to the flight chamber of the wind tunnel using an interval of 2–3 h, during which the birds were in still air with free access to a feeder and a perch. After this acclimation, the birds would sustain flight for 1 h or longer during hovering (0 $m\ s^{-1}$) and 2 $m\ s^{-1}$ and 10 min or longer during forward flight at faster velocities (4–12 $m\ s^{-1}$).

We allowed the birds to rest on the perch between trials, and we controlled access to the feeder to motivate flight. As the feeder was used in all trials, it undoubtedly affected inflow on the bird. Therefore, caution is warranted when extrapolating from our results to estimate performance in free flight. The feeder was a modified 1 ml Tuberculin syringe, 6.6 mm in diameter, with tabs removed and tip opening enlarged and painted red using fingernail polish. It was aligned parallel with inflow and suspended from the ceiling of the flight chamber using a steel wire (1.5 mm in diameter). The tip of the feeder was located in the midline of the flight chamber, approximately 10 cm back from the inlet and 20 cm down from the ceiling. Between trials, the feeder was manually refilled as necessary using Nektar-Plus or 20% sucrose. The perch was constructed of a 15 cm length of steel wire, 1.5 mm in diameter, and supported 20 cm up from the floor of the flight chamber between steel supports (12 mm×12 mm in cross section). The perch was oriented perpendicular to inflow, and at a minimum distance of 50 cm behind the tip of the feeder.

The combined frontal area of the feeder and perch (~0.008 m^2) was only 2% of the 0.36 m^2 area of the inlet of the flight chamber, so it was not necessary to correct tunnel velocity for blocking effects (Barlow et al., 1999).

Kinematics

We measured wing and body movement using digital video and three-dimensional (3D) reconstruction (Warrick and Dial, 1998; Hedrick et al., 2002). Digital video recordings, 2–4 s in duration, were obtained during longer intervals of sustained flight. We used two synchronized Redlake cameras, a PCI-2000 and PCI-500 (Redlake MASD LLC, San Diego, CA, USA) sampling at 500 frames s^{-1} and with a shutter speed of 1/2500 s. Images were stored to computer using PCI-R v.2.18 software. Flights were illuminated using four 650-W halogen lights (Lowel Tota-light, Lowel-Light Manufacturing, Inc., Brooklyn, NY, USA) distributed around the outside of the flight chamber.

We digitized anatomical landmarks and accomplished 3D reconstruction using custom M-files (available: http://www.unc.edu/~thedrick/) in MATLAB v.6.5 and v.7.0 (The Mathworks, Inc., Natick, MA, USA). To identify anatomical landmarks for digitizing, we marked the birds prior to the experiments using 1.5-mm dots of non-toxic white paint on the feathers over the spine (approximately over 1st thoracic vertebrae), dorsal and right-lateral base of tail, and, on the right wing: shoulder, wrist, distal tip of 1st secondary and distal tip of 9th primary.

For 3D reconstruction, we merged two-dimensional (2D) coordinates from each camera plane into a single 3D space using the Direct Linear Transform coefficients derived from a sixteen-point calibration frame (Hatze, 1988). For digitized points on all birds, median RMS error was <1 mm. Occasionally a point was not in the view of both cameras, resulting in a gap in the reconstructed point sequence. Point interpolation and filtering were accomplished using a quintic spline fit to known RMS error using the Generalized Cross Validatory/Spline program (Woltring, 1986).

Subsequent kinematic analysis used 3D coordinates of anatomical landmarks and software including MATLAB, IGOR Pro. (v.4.061, Wavemetrics, Inc., Beaverton, OR, USA) and Excel (v.2003, Microsoft Corp, Renton, WA, USA). We utilized a bird-centered coordinate system (*x*, *y* and *z* axes centered at shoulder) to measure kinematics relative to the body and a global-coordinate system to measure aerodynamically relevant kinematics (Gatesy and Baier, 2005; Rosén et al., 2004) that require an estimate of translation of the body due to flight velocity. We accomplished transitions between coordinate systems using translation along *x*, *y* and *z* axes and rotation about Euler angles that described body pitch about the *y* axis and yaw about the *z* axis. The anatomical landmarks we

used did not permit measurement of roll, so we assumed that no roll was present and visually inspected video samples to eliminate from analysis any intervals of flight in which the birds appeared to maneuver. Thus, the observed lateral midline of the body (Fig. 1A), between the shoulder and the base of the tail, represented the mid-frontal plane, and the dorsal mid-line of the body, between the spine and the base of the tail, represented the mid-sagittal plane.

Movement at the wrist was used to identify characteristic portions of wingbeats including the transitions between upstroke and downstroke and the middle of upstroke and downstroke. At the start of each half-stroke, wrist span began increasing (the wrists were abducted from the mid-sagittal plane of the body). Downstroke started with wrist depression and upstroke began with wrist elevation. Mid-half-strokes occurred as the wristspan was at a local maximum, and with wrist elevation at the mid-frontal plane of the body. Body angle (β, deg.) was the acute angle between horizontal and the mid-frontal plane of the body (Fig. 1A). The stroke plane of the wing connected the shoulder, wingtip at start of downstroke and wingtip at the end of downstroke. We measured 'anatomical' stroke-plane angle (Gatesy and Baier, 2005) relative to the mid-frontal plane of the body (γ_b, deg.) and a 'tracking' stroke plane angle relative to the horizontal plane (γ_h, deg.). Wing chord was a line connecting the wrist and the distal tip of the 1st secondary, and chord angle (α_c, deg.) was the cranially oriented acute angle formed between this lead line and the mid-frontal plane of the bird. This angle was $<0°$ for pronation and $>0°$ for supination.

We calculated wing and wrist span (mm) as double the perpendicular distance between the line connecting the spine and dorsal base of tail (hereafter 'dorsal midline') and the distal tip of the 9th primary or the wrist, respectively. Span ratios for the wingtips and wrists (dimensionless) were spans at mid-upstroke divided by spans at mid-downstroke.

The inverse of the duration of the wingbeat gave wingbeat frequency (f, Hz). Wingbeat amplitude (ϕ, deg.) was measured in the bird-centered coordinate system as the acute angle formed between the line connecting the shoulder and wingtip at the start of downstroke and the line connecting the shoulder and the distal wingtip at the end of downstroke. Duration (s) of downstroke and upstroke were used to compute the proportion of time spent in downstroke (%). Average angular velocity of the wing (rad s^{-1}) was ϕ divided by duration of each downstroke or upstroke.

Free-stream velocity (V) in the wind tunnel and an estimate of the vertical component of induced velocity (V_i) were incorporated into certain kinematic measurements. Angle of attack of the wing (α, deg.) was the angle between wing chord and resultant velocity summed from wing-flapping velocity, free-stream air velocity in the wind tunnel, and V_i. The 3D flow field in the vicinity of the wings and body of a hummingbird is complex (Warrick et al., 2005) and a reasonable estimate of instantaneous near-field flow (Sane, 2006) was beyond the scope of the present study. As a simple first approximation, we calculated V_i using Rankine–Froude momentum-jet theory,

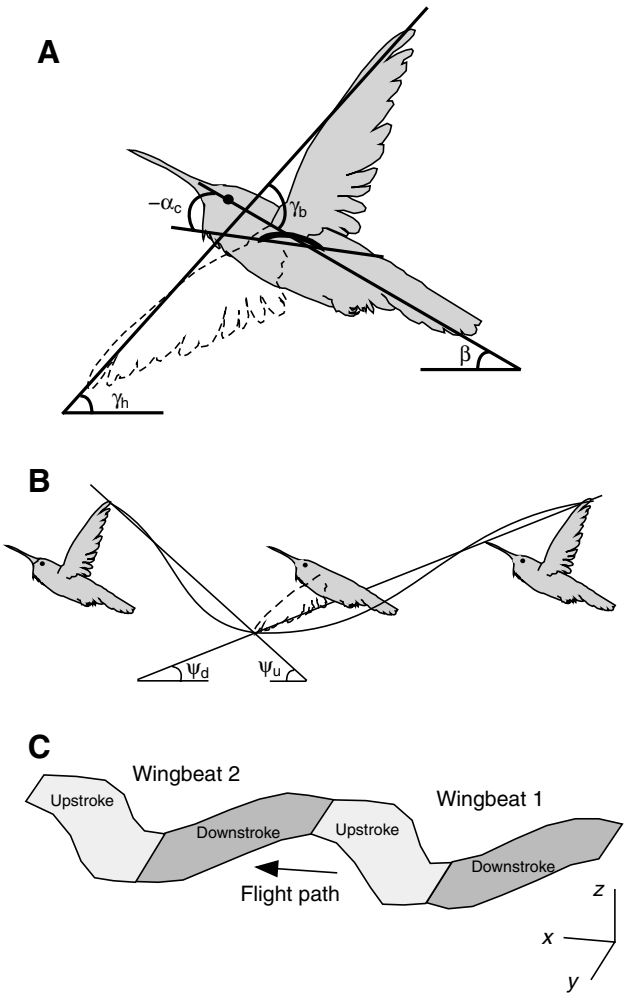

Fig. 1. Angles and areas measured from wing and body motion of rufous hummingbirds (*Selasphorus rufus*) during flight. Certain measures were bird-centered (A) and those in (B,C) were derived from global coordinates because they incorporated free-stream velocity. Filled-outlines of bird (A,B) illustrate wing at the start of downstroke, and broken-outline of wing illustrates wing position at the end of downstroke. (A) Black cross-section represents a pronated wing at mid-downstroke. α_c=chord angle relative to mid-frontal plane of body with $\alpha_c>0$ for supination and $\alpha_{c<}0$ for pronation. β=body angle relative to horizontal. γ_b=anatomical stroke-plane angle relative to mid-frontal plane of body. γ_h=tracking stroke-plane angle relative to horizontal. (B) ψ_d and ψ_u=global stroke-plane angle during downstroke and upstroke, respectively. (C) Global stroke-plane area was outlined by the wingtips during downstroke (dark gray areas) and upstroke (light gray areas) for each wingbeat.

treating the wings as an actuator disc (Pennycuick, 1975). For hovering:

$$V_i = (M_b \boldsymbol{g} / 2\rho S_d)^{-0.5}, \quad (1)$$

and, for forward flight:

$$V_i = M_b \boldsymbol{g} / 2V\rho S_d, \quad (2)$$

where M_b=body mass, $\boldsymbol{g}$=gravitational acceleration, ρ=air

Table 2. *Variation in bird-centered kinematics among flight velocities (0–12 m s^{-1}) in the rufous hummingbird (Selasphorus rufus)*

Variable	Value	*F*	*P*
Body angle, β (deg.)	24±15	68.1	<0.0001
Anatomical stroke-plane angle, γ_b (deg.)	67±8	19.0	<0.0001
Tracking stroke-plane angle, γ_h (deg.)	43±21	182.4	<0.0001
Chord angle, α_c (deg.)			
Mid-downstroke	–26±8	3.3	0.0168
Mid-upstroke	56±29	19.4	<0.0001
Wingbeat frequency *f* (Hz)	41±1	1.9	0.1183
Wingbeat amplitude (deg.)	107±9	3.1	0.0202
Downstroke (%)	50±2	4.8	0.0024
Angular velocity (rad s^{-1})			
Downstroke	155±16	4.2	0.005
Upstroke	156±19	6.2	0.0005
Wingspan (mm)			
Mid-downstroke	99±3	5.2	0.0014
Mid-upstroke	92±2	1.2	0.3554
Wristspan (mm)			
Mid-downstroke	54±1	1.9	0.116
Mid-upstroke	52±1	1.4	0.2424
Span ratio (%)			
Wingtips	93±3	3.9	0.0072
Wrists	98±1	2.8	0.0332

Values are mean ± s.d. among flight velocities (*N*=7), using *N*=5 birds per velocity.
Statistical significance of the effect of velocity, *F* and *P* values are from repeated-measures analysis of variance (d.f. 4, 6).

density, which averaged 1.15 kg m^{-3} during the experiments, and S_d was measured as the horizontal projection of the bird-centered stroke plane area (Wakeling and Ellington, 1997):

$$S_d = \phi l^2 \cos\gamma_h , \quad (3)$$

where *l*=wing length. We translated bird-centered coordinates along the *x* axis, according to flight velocity and time (Fig. 1B,C), so that we could measure 'global' angle between the stroke-plane and horizontal for downstroke (ψ_d) and upstroke (ψ_u) and 'global' stroke-plane area (mm^2) outlined by the wingtips during each half stroke.

Statistical analyses

For each kinematic variable, we computed the mean value within each bird (*N*=5–10 wingbeats) for each velocity (*N*=7). We then used these means to test for a significant effect of flight velocity upon each variable using a univariate repeated-measures ANOVA (d.f. 4, 6) and StatView v.5.0.1 (SAS Institute, Inc., Cary, NC, USA). We also computed an overall mean ± s.d. among the 7 flight velocities.

To describe variation in α_c and α within wingbeats, we converted time within a wingbeat cycle into a percentage of the full cycle that began with the start of downstroke and ended with the start of the subsequent downstroke. We then interpolated observed α_c and α using cubic-spline fitting with 100 points per curve. We computed an average and s.d. among birds for each of the 100 points.

Values are presented as means ± s.d.

Results

Hummingbirds accomplished flight at different velocities by significantly varying the majority (75%) of the bird-centered kinematics variables that we measured (Table 2, Fig. 2).

Dorsal and lateral projections of the paths of the wingtips and wrists revealed gradual changes across the range of velocities (Fig. 2). During upstroke of slow flight (0 and 2 m s^{-1}), the tips and wrists traced in reverse nearly the same paths that were exhibited during downstroke. Lateral views of the paths at these slow flight velocities reveal an upwardly concave path of the wrists and wingtips, with the path of the wingtips also describing a horizontal figure-8 pattern in which the tip was higher during early downstroke, dipped down during late downstroke, raised at the start of upstroke, and dipped low during mid- and late upstroke. Wing movement at flight velocities of 4–12 m s^{-1} created two patterns. In dorsal view, the path of the wrists, but especially the wingtips, described a figure-8 loop with maximal wing span always exhibited during the middle of downstroke, and with the figure-8 loops becoming progressively more obvious as velocity increased. In lateral view, the paths of the wrists and wingtips were ellipses, with the wrists and wingtips positioned more cranially during downstroke and more caudally during upstroke.

As flight velocity increased from 0 to 12 m s^{-1}, body angle (β) decreased from 50±2° to 13±5° and tracking stroke-plane angle (γ_h) increased from 15±4° to 68±5° (Fig. 3A). These changes in β and γ_h produced a minimum anatomical stroke-

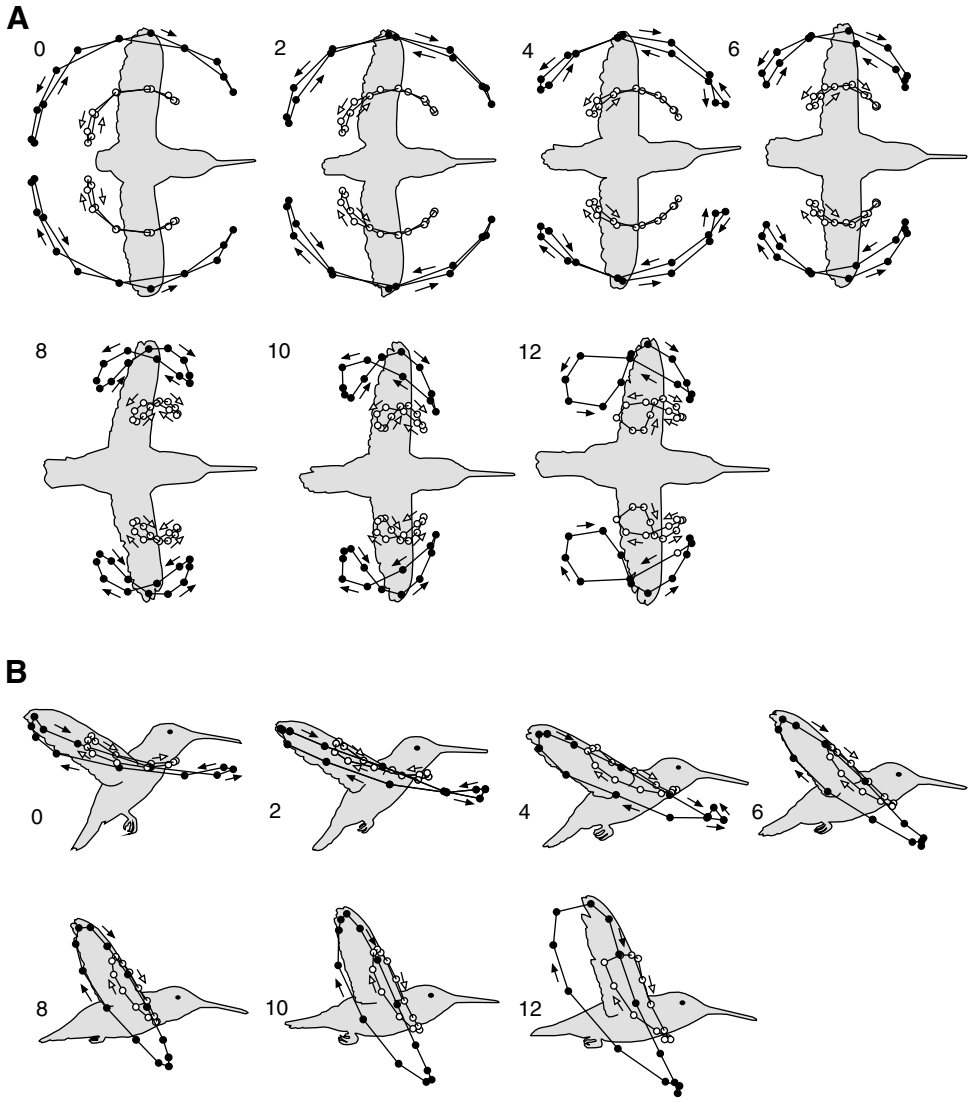

Fig. 2. Wing motion relative to the body of a rufous hummingbird (*Selasphorus rufus*) flying at velocities of 0–12 m s^{-1}. (A) Dorsal view with bird silhouette at mid-downstroke. As we measured kinematics only from the right wing, paths for the left-wing are mirror images. (B) Lateral view with bird silhouette at start of downstroke. Black circles indicate position of wingtips, and white circles indicate position of wrists. Paths of wing motion are from 3D measurements, so circles within the paths are synchronized for a given velocity. Circles and arrows indicate sequential position and local direction of movement.

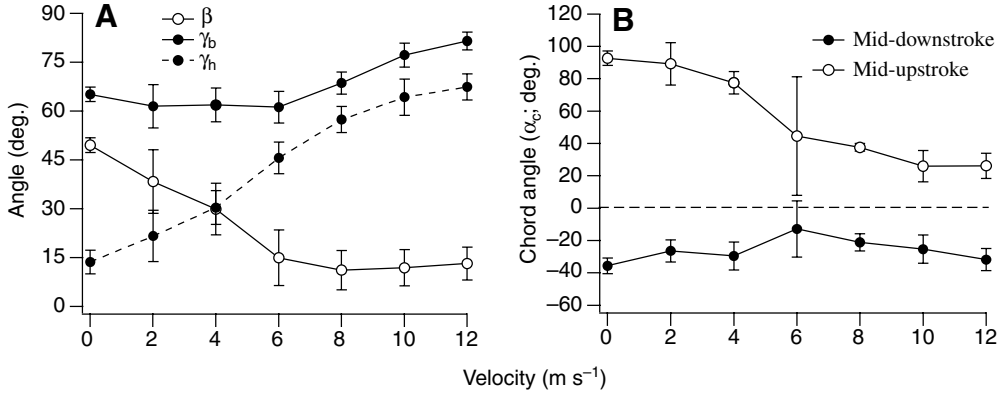

Fig. 3. Angles describing bird-centered wing and body kinematics in rufous hummingbirds (*Selasphorus rufus*, *N*=5) flying at velocities 0–12 m s^{-1}. (A) Body angle relative to horizontal (β), tracking stroke-plane angle relative to horizontal (γ_h) and anatomical stroke-plane angle relative to mid-frontal plane of body (γ_b). (B) Chord angle of wing relative to mid-frontal plane of body (α_c) at mid-downstroke and mid-upstroke. Values are means ± s.d.

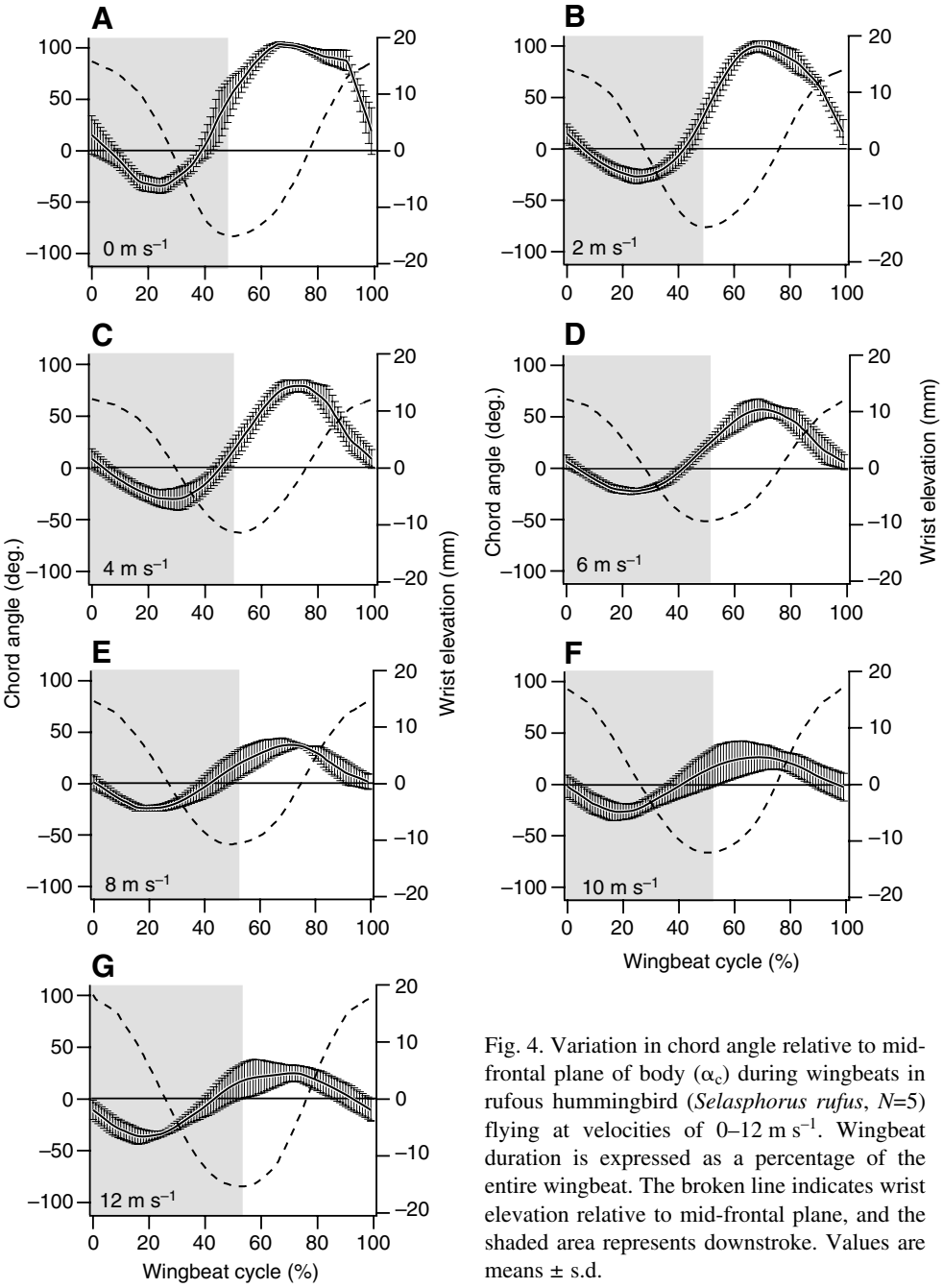

Fig. 4. Variation in chord angle relative to mid-frontal plane of body (α_c) during wingbeats in rufous hummingbird (*Selasphorus rufus*, *N*=5) flying at velocities of 0–12 m s^{-1}. Wingbeat duration is expressed as a percentage of the entire wingbeat. The broken line indicates wrist elevation relative to mid-frontal plane, and the shaded area represents downstroke. Values are means ± s.d.

plane angle (γ_b) of 61±5° during flight at 6 m s^{-1} and a maximum γ_b of 82±3° during flight at 12 m s^{-1}.

Chord angle (α_c) varied significantly among flight velocities, with P=0.0168 for α_c at mid-downstroke and P<0.0001 for α_c at mid-upstroke (Table 2, Fig. 3B). Pronation of the wing, relative to the mid-frontal plane, of the body, occurred through most of downstroke. Consequently, α_c was negative during the majority of this phase of the wingbeat. Regardless of flight velocity, at the start of downstroke, α_c was near 0°, reached a minimum of between –13±17° and –36±5° at mid-downstroke, and returned to 0° at approximately 40% of the wingbeat cycle, 10% of the cycle duration before the onset of upstroke (Fig. 4).

In contrast with downstroke, the wing was supinated during most of upstroke, resulting in positive values of α_c. Peak positive values of α_c were exhibited at mid-upstroke, at a time 65–70% into the full wingbeat cycle. Mid-upstroke α_c decreased with increasing flight velocity from a maximum of 93±4° during hovering (0 m s^{-1}) to 26±10° and 26±8° during flight at 10 and 12 m s^{-1}.

Interactions among frequency (f), amplitude (ϕ), and the percentage of the wingbeat cycle spent in downstroke produced significant variation in the angular velocity of the wing among flight velocities (Fig. 5). With an average of 41±1 Hz, f was among the minority of bird-centered kinematics that did not vary significantly with flight velocity (P=0.1668). Wingbeat amplitude (ϕ) varied according to a U-shaped curve, with ϕ between 100±6 and 103±19° at velocities of 2–8 m s^{-1} and ϕ from 109±12 to 126±12° at 0, 10 and 12 m s^{-1}. The percentage of the wingbeat spent in downstroke increased with increasing flight velocity from 48% at 0 and 2 m s^{-1} to 53±1% at 12 m s^{-1}. For both downstroke and upstroke, the angular velocity of the wing varied with velocity according to U-shaped curves. Average angular velocity among all flight velocities was similar between downstroke (155+16 rad s^{-1}) and upstroke (156+19 rad s^{-1}). Local minima and maxima for each half of the wingbeat cycle occurred at different velocities. Specifically, angular velocity during downstroke varied from 140±6 rad s^{-1} at 8 m s^{-1} to 178±21 rad s^{-1} at 0 m s^{-1}, while minimum angular velocity during upstroke was 134±24 rad s^{-1} at 4 m s^{-1} and maximum was 195±23 rad s^{-1} at 12 m s^{-1}.

All variables related to wing and wrist spans exhibited relatively low variability among flight velocities (Table 2); nevertheless, velocity had a significant effect upon wingspan at mid-downstroke (P=0.0014) and the span ratios of the wingtips (P=0.0072) and wrists (P=0.0332). At mid-downstroke, wingspan was slightly less during flight at 0 and 2 m s^{-1} (93±3 mm and 95±5 mm, respectively) compared with

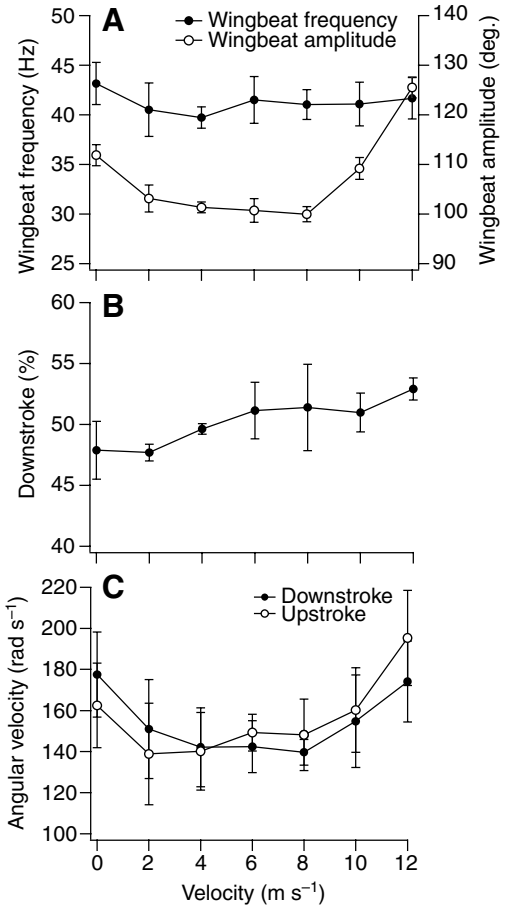

Fig. 5. (A) Wingbeat frequency and amplitude (ϕ), (B) proportion of wingbeat spent in downstroke and (C) average angular velocity of the wing, during downstroke and upstroke during flight in rufous hummingbirds (*Selasphorus rufus*, *N*=5) flying at velocities of 0–12 m s^{-1}. Values are means ± s.d.

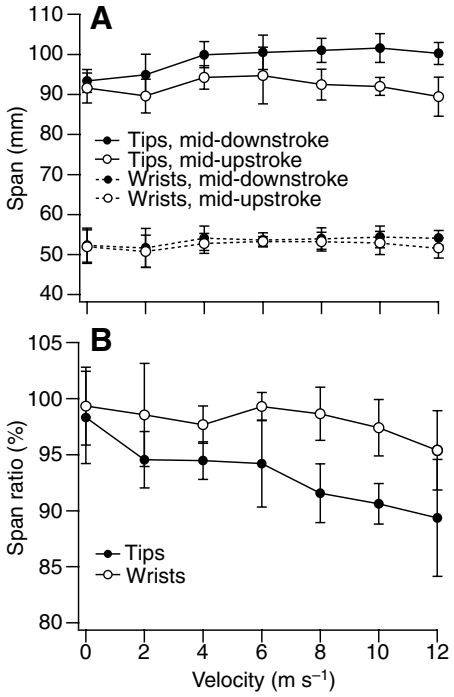

Fig. 6. (A) Wingspan and wristspan during mid-downstroke (black circles) and mid-upstroke (white circles) and (B) span ratio in rufous hummingbirds (*Selasphorus rufus*, *N*=5) flying at velocities of 0–12 m s^{-1}. Values are means ± s.d.

flight at velocities of 4–12 m s^{-1}, where mid-downstroke spans were between 100±3 mm and 102±4 mm. In general, span ratio for the wingtips and the wrists decreased as flight velocity increased. A minor deviation from this overall pattern was an observed increase in average span ratio of the wrist from 98±2 to 99±1% between 4 and 6 m s^{-1}. Among flight velocities, span ratio for the wrists was greater (98±1%) than for the wingtips (93±3%).

All of the measured global-coordinate wing kinematics varied significantly with flight velocity (Table 3; Figs 7–9). Dorsal and lateral projections of the paths of the wingtips and wrists revealed that overlap in wrist and tip excursion occurred between subsequent downstrokes at 0 and 2 m s^{-1}, and overlap in the paths of the wingtips was also apparent at 4 m s^{-1}. At each flight velocity, downstroke covered a larger area than upstroke. However, the difference between the means was less than 1 s.d. during hovering and was accounted for solely by slight flexion of the wings during upstroke, with span ratio of 98±4% (Fig. 6B). Downstroke plane area increased uniformly

Table 3. *Variation in global-coordinate wing kinematics among flight velocities (0–12 m s^{-1}) in the rufous hummingbird (Selasphorus rufus)*

Variable	Value	*F*	*P*
Downstroke-plane angle, ψ_d (deg.)	20±4	15.4	<0.0001
Upstroke-plane angle, ψ_u (deg.)	88±53	551.5	<0.0001
Downstroke-plane area (mm^2)	10945±4242	150.2	<0.0001
Upstroke-plane area (mm^2)	6330±2588	146.9	<0.0001
Angle of attack, α (deg.)			
Mid-downstroke	14±1	4.4	0.0038
Mid-upstroke	9±22	22.0	< 0.0001

Values are mean ± s.d. among flight velocities (*N*=7), using *N*=5 birds per velocity.
Statistical significance of the effect of velocity, *F* and *P* values are from repeated-measures analysis of variance (d.f. 4, 6).

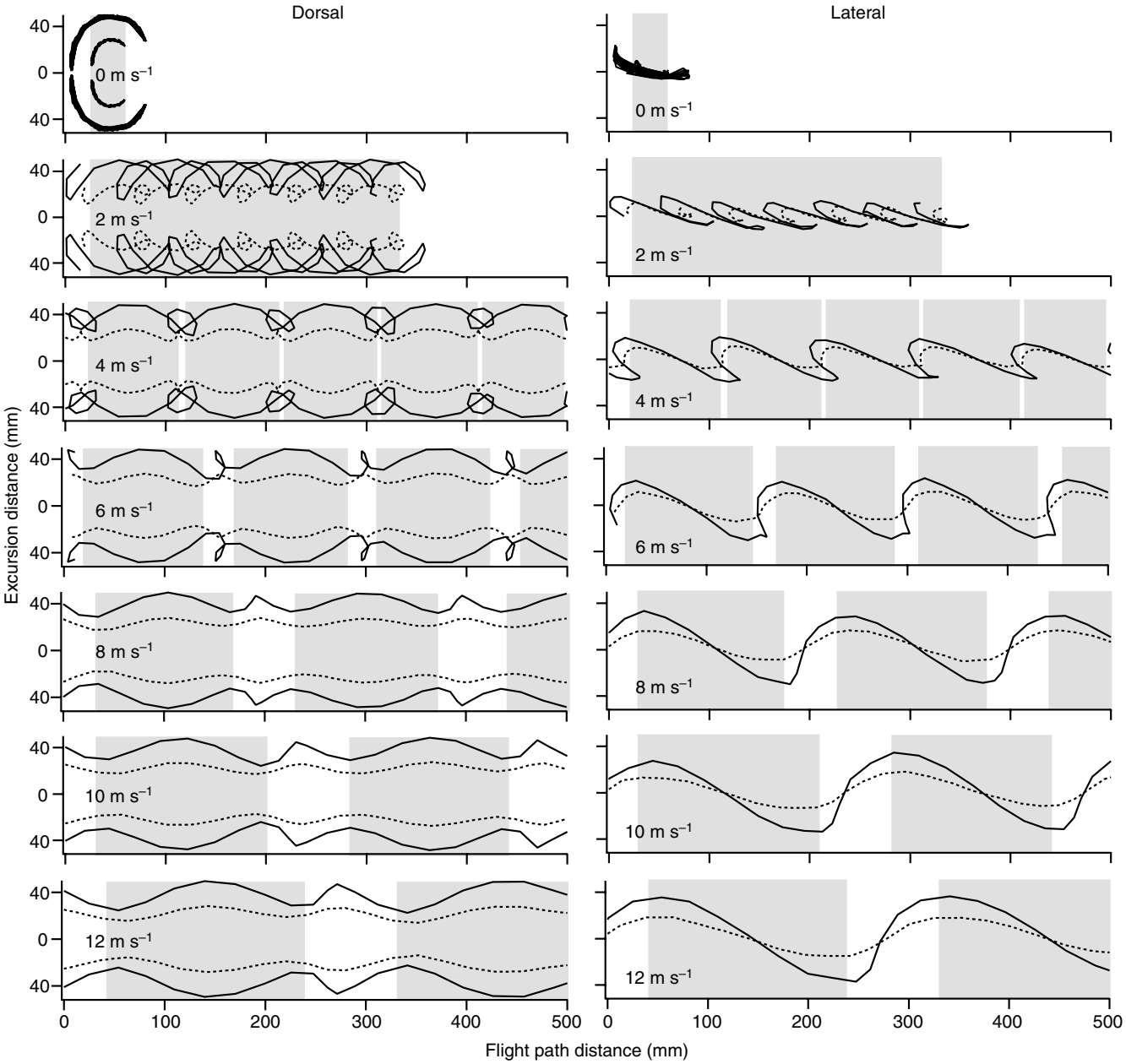

Fig. 7. Dorsal and lateral views of wingtip and wrist paths with translation due to free-stream velocity (*V*) and time. These data are from a rufous hummingbird (*Selasphorus rufus*) flying at velocities of 0–12 m s^{-1} (same subject as in Fig. 2). All *x*-axes represent 500 mm along a flight path. Solid line=wingtip, dotted line=wrist. Shaded regions indicate downstroke as defined using wrist motion. For each downstroke, wingtip excursion exceeded wrist excursion in all dimensions, so the shaded regions would be enlarged if downstroke were based on motion of the wingtip.

with velocity from 3059±411 mm^2 at 0 m s^{-1} to 15296±1370 mm^2 at 12 m s^{-1}. Upstroke-plane area was 2830±380 mm^2 during hovering, approximately 4700 mm^2 during flight at 2–4 m s^{-1}, and increased with increasing velocity to reach a maximum of 10011±278 mm^2 during flight at 12 m s^{-1}.

Along with changes in stroke plane area (Fig. 7 and Fig. 8A), the angle of the aerodynamic stroke plane changed with velocity (Fig. 7 and Fig. 8B). A slight increase in ψ_d occurred as velocity increased, with a mimimum of 14±4° during flight at 2 m s^{-1} increasing to 23° during flight from 8 to 12 m s^{-1}. In dramatic contrast, ψ_u decreased with each incremental increase in velocity, from 162±4° during hovering to 35±3° during flight at 12 m s^{-1}.

Angle of attack (α) varied among velocities and within wingbeats (Table 3; Fig. 8C and Fig. 9). Mid-downstroke α was greatest during hovering (23±5°), decreased with increasing velocity, and varied from 11–13° during faster flight (6–12 m s^{-1}). During mid-upstroke of flight at 0 and 2 m s^{-1}, α was negative, indicating an inverted airfoil (i.e. with the curved, anatomical underside of the wing facing in the same direction as presumed low pressure above the wing), whereas

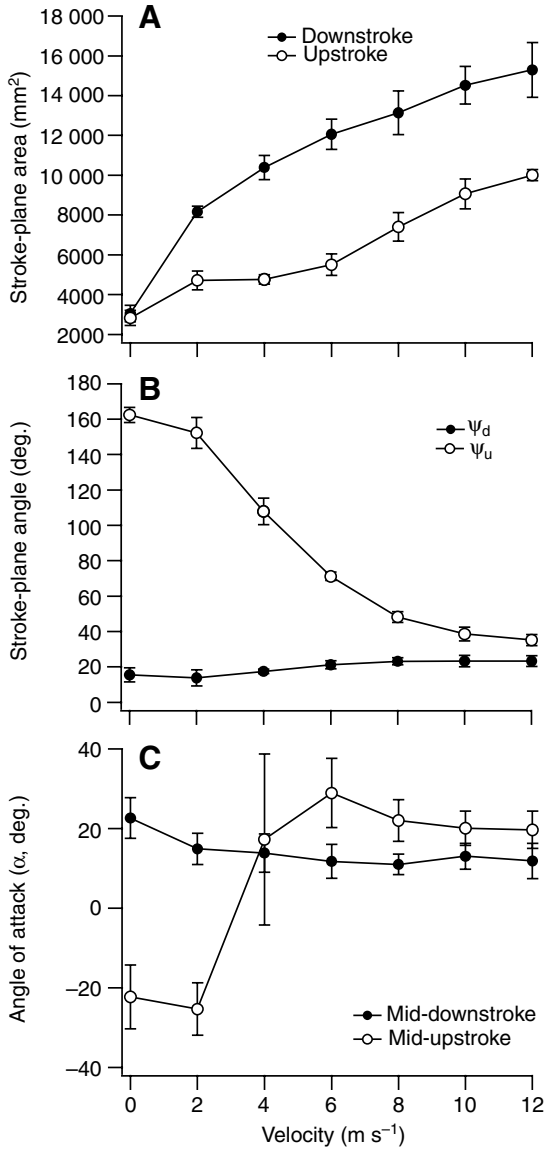

Fig. 8. Kinematic variables derived using free-stream velocity (V) and induced velocity (V_i) for rufous hummingbirds (*Selasphorus rufus*, N=5) flying at velocities of 0–12 m s^{-1}. (A) Global stroke-plane area for downstroke and upstroke. (B) Global stroke-plane angle for downstroke (ψ_d) and upstroke (ψ_u). (C) Angle of attack of the wing (α) at mid-downstroke and mid-upstroke.

α was positive at mid-upstroke during flight from 4 to 12 m s^{-1}. Negative values for mid-upstroke α produced an overall mean among flight velocities (9±22°) that was atypical of any given velocity. Ignoring which surface of the wing was uppermost, $|\alpha|$ was more useful as an average descriptor of the relative direction of incurrent air; mid-upstroke $|\alpha|$ averaged 22±4°. Average α at mid-downstroke 14±1°.

Within wingbeats, α varied more during slow flight (0 and 2 m s^{-1}) compared with flight at 4–12 m s^{-1} (Fig. 9). For example, α ranged from –32±14° to 56±7° during flight at 0 m s^{-1}, and from 11±4° to 33±11° during flight at 12 m s^{-1}. During hovering, α varied between downstroke and upstroke approximately in a symmetrical manner about 0°. At the middle of each half stroke, $|\alpha|$ was 22–23°. Negative α was exhibited from slightly before the end of downstroke (44% of wingbeat cycle) to slightly before the end of upstroke (93% of cycle). The interval of negative α was more contracted in duration at 2 m s^{-1} and occurred during the middle of upstroke, between times at 62% and 87% of the full cycle. Peak positive α was exhibited during early downstroke of flight at 0 m s^{-1}, 9% into the wingbeat cycle. In contrast, for all other flight velocities, peak positive α was exhibited at 51–58% of the wingbeat cycle, concurrent with, or slightly after, the transition between downstroke and upstroke.

Discussion

Our experiments revealed that hummingbirds change a variety of bird-centered kinematic parameters among flight velocities and within wingbeats (Table 2, Figs 2–6), which causes changes in global-coordinate variables that are likely relevant to their aerodynamic performance (Table 3; Figs 7–9). Thus, our experiments provide new details about wing kinematics that should help improve understanding of hummingbird flight.

Three of the patterns that we observed were consistent with the kinematics previously reported for ruby-throated hummingbirds (Greenewalt, 1960a; Greenewalt, 1960b): f did not vary significantly among flight velocities (Table 2, Fig. 5A), while β and γ_h exhibited significant variation. The lack of variation in f among flight speeds is also consistent with hummingbird behavior during hovering. When adjusting to varying power demands of load lifting or hovering in hypodense air, hummingbirds modulate ϕ to a much greater degree than f (Chai and Dudley, 1995; Chai et al., 1997; Chai and Millard, 1997; Altshuler and Dudley, 2002; Altshuler and Dudley, 2003).

A mechanical oscillator hypothesis has been proposed for modeling hummingbird wing motion (Greenewalt, 1960a; Greenewalt, 1960b). This describes the wing as a damped, driven oscillator, and one prediction from the model is that $fl^{5/4}$is constant. Among flight velocities studied here, this product did not vary significantly using f and mid-downstroke l (F=1.779, P=0.1461, d.f. 4, 6), or using f and mid-upstroke l (F=0.888, P=0.5188, d.f. 4, 6). Thus, our results provide support for the hypothesis, and demonstrate how hummingbirds modulate the orientation and trajectory of their mechanical oscillator to accomplish a change in velocity. Additional tests of the assumptions of the hypothesis are necessary, however, including the contribution of profile drag to damping and whether muscle force is proportional to strain (Greenewalt, 1960b).

Insight into muscle force production is also necessary to evaluate whether the U-shaped curve exhibited for angular velocity of the wing (Fig. 5C) is representative of the shape of the mechanical power curve for hummingbird flight. If muscle force is proportional to strain, as assumed by the mechanical oscillator hypothesis (Greenwalt, 1960b), and strain in the primary flight muscles is proportional to ϕ (Fig. 5A), our

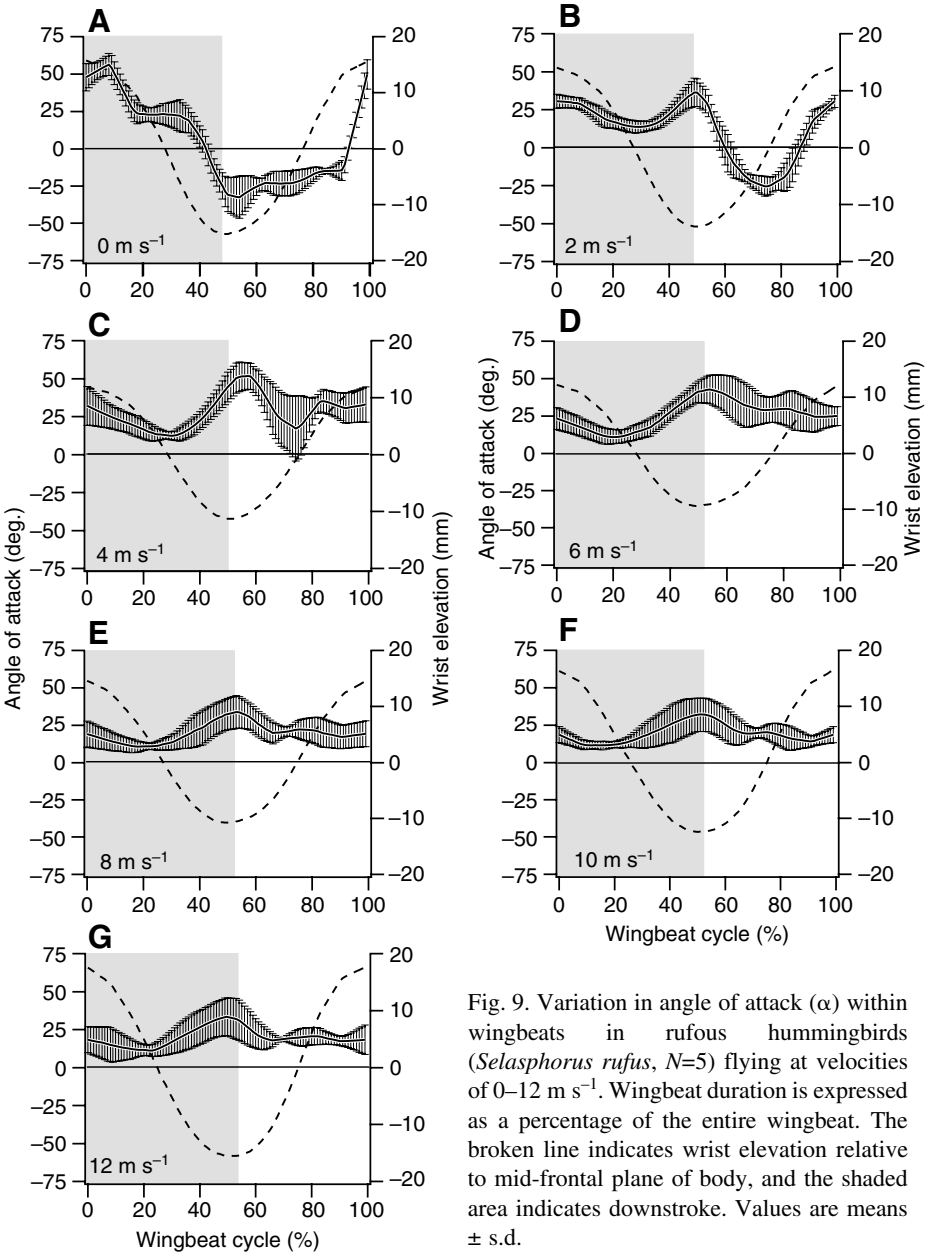

Fig. 9. Variation in angle of attack (α) within wingbeats in rufous hummingbirds (*Selasphorus rufus*, *N*=5) flying at velocities of 0–12 m s^{-1}. Wingbeat duration is expressed as a percentage of the entire wingbeat. The broken line indicates wrist elevation relative to mid-frontal plane of body, and the shaded area indicates downstroke. Values are means ± s.d.

including the rock dove (*Columba livia*, hereafter 'pigeon') and cockatiel (Brown, 1953; Brown, 1963; Scholey, 1983; Tobalske and Dial, 1996; Tobalske, 2000; Tobalske et al., 2003a). Hummingbirds also share with pigeons characteristics of wing motion apparent in faster flight, specifically with the tips and wrists following an elliptical trajectory in lateral view and a figure-8 trajectory in dorsal view (Tobalske and Dial, 1996) (Fig. 2B).

The wing paths that hummingbirds share with other, distantly related species highlights that the evolution and functional significance of the wingtip-reversal upstroke used by other species merits additional study. Flow visualization shows that the upstroke in hovering hummingbirds, featuring negative angle of attack and chord angle (α and α_c; Figs 3–5), provides 25% of the weight support required from a full wingbeat cycle (Warrick et al., 2005). In comparison, some studies suggest that the tip-reversal upstroke of other bird species is an aerodynamically inactive recovery stroke (Spedding et al., 1984; Hedrick et al., 2004), while others indicate that the proximal wing may continue to support body weight while the distal wing provides thrust (Corning and Biewener, 1998; Usherwood et al., 2003; Usherwood et al., 2005). An extended, tip-reversed wing may also facilitate maneuvering at low speeds (Warrick and Dial, 1998). At present, the relationship between tip reversal and the phylogeny of birds is unknown, but it is possible that a tip-reversal upstroke may represent a precursor style of wing movement that an ancestral form exhibited early during the evolution of hovering within the Trochilidae.

kinematic data indicate that the mechanical-power curve for hummingbird flight has a pronounced U-shape, similar to curves exhibited by other bird species (Tobalske et al., 2003a).

The general pattern of bird-centered wingtip paths in lateral projection (Fig. 2B) was similar to that reported for ruby-throated hummingbirds (Greenewalt, 1960a), but our data furnish new insight into lateral-projections of wrist motion as well as the path followed by the tips and wrists in dorsal projection (Fig. 2A). Changing velocity of flight in the wind tunnel in 2 m s^{-1} increments resulted in gradual but consistent shifts in wingtip and wrist paths. The figure-8 path of the tips that was apparent in lateral view at 0 and 2 m s^{-1}, and, to a lesser extent, during flight at 4 m s^{-1}, is similar to that exhibited during slow flight by other bird species that possess pointed wings or wings of relatively high aspect ratio (*AR*=5.5–7),

Our measurements of α_c indicated continuous variation within (Fig. 4) and among (Table 2, Fig. 3B) flight velocities. Contrary to an expectation from earlier reports (Stolpe and Zimmer, 1939; Greenewalt, 1960a; Greenewalt, 1960b) that the two halves of the hovering wingbeat would be symmetrical, mirror images of one another, $|\alpha|$ during upstroke and downstroke exhibited greater disparity at slow velocity (0–4 m s^{-1}) than during faster flight (6–12 m s^{-1}). The only comparable values of α_c are available for zebra finch at mid-downstroke (Tobalske et al., 1999), and the coefficient of variance (CV=s.d./mean) for α_c at mid-downstroke is greater in hummingbirds (29%) than in zebra finch (17%).

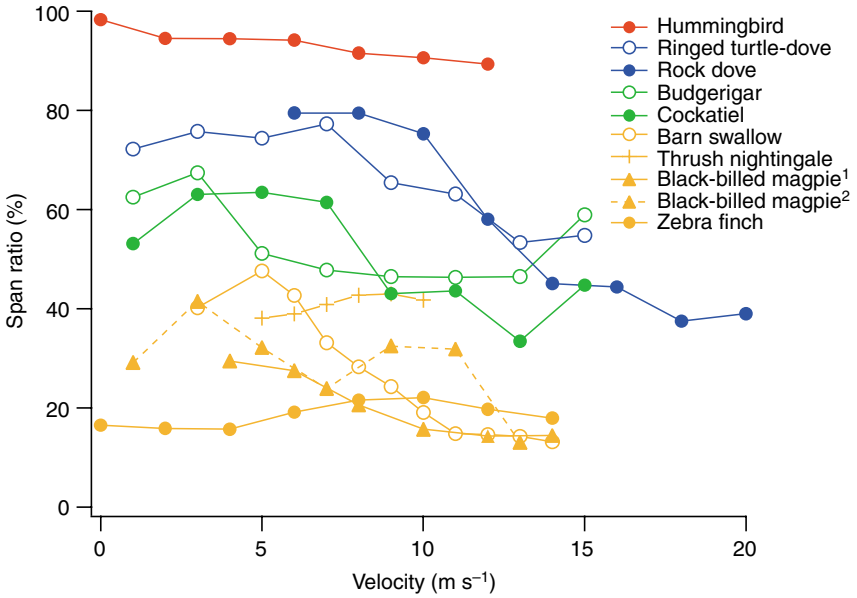

Fig. 10. Wingspan ratio as a function of flight velocity compared among bird species. Values shown are means. Colors indicate species within the same order: Red=Trochiliformes, rufous hummingbird *Selasphorus rufus* (this study); blue=Columbiformes, ringed turtle-dove *Streptopelia risoria* (Tobalske et al., 2003b) and rock dove ('pigeon') *Columba livia* (Tobalske and Dial, 1996); green=Psittaciformes, budgerigar *Melopsittacus undulatus* and cockatiel *Nymphicus nymphicus* (Tobalske et al., 2003b); orange=Passeriformes, barn swallow *Hirundo rustica* (Park et al., 2001), thrush nightingale *Luscinia luscinia* (Rosén et al., 2004), black-billed magpie *Pica hudsonica* [1]Tobalske and Dial (Tobalske and Dial, 1996), [2]Tobalske et al. (Tobalske et al., 2003b) and zebra finch *Taeniopygia guttata* (Tobalske et al., 1999).

Zebra finch use an extremely different flight style compared with rufous hummingbirds (Tobalske et al., 1999; Tobalske et al., 2005a), and further comparison illustrates that the relative magnitude of variation for a given bird-centered kinematic variable differs between these two species depending upon the variable under consideration. Zebra finch have low-aspect ratio, rounded wings (*AR*=4.5), regularly flex their wings to adduct them almost against their body on upstroke (average span ratio=19%) and regularly use intermittent bounds (40–45% of total time during fast flight). Compared with zebra finch (Tobalske et al., 1999), hummingbirds exhibited greater variation in the percentage of their wingbeat spent in downstroke (CV=8% *vs* 3%), γ_h (CV=48% *vs* 24%) and γ_b (CV=12% *vs* 4%). In contrast, variation is greater in zebra finch for f (CV=5% *vs* 2%), ϕ (CV=15% *vs* 8%), β (CV=45% *vs* 12%), and wingspan at mid-upstroke (CV=13% *vs* 2%). Angular velocity of the wing during downstroke exhibits a CV of 11% in both species.

A comprehensive comparative analysis for all of these kinematic parameters awaits further study; however, one pattern that readily emerges from the data available for these and other bird species is that hummingbirds exhibit the highest span ratio, and the lowest variation in span ratio, of any species studied to date (Fig. 10). Their wingtip span ratio averaged 93% among velocities, and span ratios in other species vary from 17% to 80% (Tobalske and Dial, 1996; Park et al., 2001; Tobalske et al., 2003b; Rosén et al., 2004). Although this supports the view that hummingbirds have a kinematically 'rigid' wing, broadly consistent with the mechanical oscillator hypothesis (Greenewalt, 1960a; Greenewalt, 1960b), a span ratio of less than 100% is evidence that they flex their wings on upstroke (Fig. 2A, Fig. 6 and Fig. 7).

Given that average wingtip span ratio in rufous hummingbirds was less than wrist span ratio (Table 2; Fig. 6), it appears that the majority of wing flexion during upstroke in hummingbirds occurs at the wrist, rather than at the shoulder or elbow. Further, the decrease in tip span ratio with flight velocity was, in roughly equal measure, a result of increased wrist flexion during upstroke, and increased extension during downstroke. The increase in downstroke span with increasing forward flight velocity may have allowed for the greater translational velocity required for a useful α, as the vector of incident air becomes increasingly dominated by forward flight velocity (V). The change in span ratio may also provide new insight into the functional morphology of the muscular and skeletal elements of the hummingbird wing, which feature a proportionally short humerus and long distal (hand wing) bones (Stolpe and Zimmer, 1939; Greenewalt, 1960a). Hummingbirds also have exaggerated curvature of their radius and ulna that is hypothesized to accommodate proportionally large muscles to control extension, flexion and long-axis rotation of the hand wing (Dial, 1992b).

Species that are closely related to each other, hypothesized to be within the same avian order (Sibley and Ahlquist, 1990), appear to group similarly according to their characteristic span ratios (Fig. 10). Fully testing phylogenetic influences (Felsenstein, 1985; Garland et al., 1992) on this pattern relative to wing design is beyond the scope of our present analysis. Regardless of aspect ratio or wing shape, there is a general trend to decrease span ratio with increasing velocity among the rufous hummingbirds studied here, as well as in previously studied Columbiformes (pigeons and ringed turtle doves *Streptopelia risoria*), Psittaciiformes (budgerigars *Melopsittacus undulatus* and cockatiels) and two species of Passeriformes [barn swallows *Hirundo rustica* and black-billed magpies *Pica hudsonica* (Tobalske and Dial, 1996; Park et al., 2001; Tobalske et al., 2003b)]. This trend may be explained by the need to limit negative thrust during a lifting upstroke at fast velocities (Rayner, 1986; Rayner, 1988; Tobalske, 2000; Hedrick et al., 2002). Two passerine species, the zebra finch and thrush nightingale (*Luscinia luscinia*), exhibit an increase in span ratio with increasing velocity (Tobalske et al., 1999;

Rosén et al., 2004). At least for the zebra finch, we predict the increase in span ratio is due to an effort on the part of the bird to enhance weight support by moving toward a lifting upstroke because the bird can potentially use intermittent bounds to offset an increase in average thrust requirements as velocity increases (Tobalske et al., 1999).

Other than a report of 'undulating' during flight (Murphy, 1913), there have been no published accounts of hummingbirds using intermittent flight. Given the widespread use of this flight style in other species of small birds (Rayner, 1985, Tobalske, 2001), it is therefore noteworthy that two of the five birds in our study regularly used intermittent glides and bounds when flying at velocities between 8 and 12 m s^{-1} (94±9% of their total number of flights at these velocities).

Continuous variation in angle of attack (α) within wingbeats (Fig. 9) indicated that bound circulation on the wing is likely to vary throughout the wingbeat cycle of hummingbirds, and this variation should be evident in the wake as cross-stream starting and stopping vortices that parallel the long axis of the wings (Rayner, 1986; Rayner, 1988; Tobalske, 2000). We interpret that this will give rise to some form of 'ladder' appearance in the wake similar to the structure described for the wake of the thrush nightingale during fast forward flight (Spedding et al., 2003). Our ongoing research into the wake of flying hummingbirds using digital particle image velocimetry (DPIV) appears to support this expectation (Tobalske et al., 2005b; Warrick et al., 2005).

Relative to incurrent air, the wing functioned as an inverted airfoil during the upstroke of flight at 0 and 2 m s^{-1}. The opposite sign, nearly symmetrical pattern of α between the two halves of the wingbeat cycle during hovering would appear to support a hypothesis that the two halves of the wingbeat are functionally identical (Stolpe and Zimmer, 1939; Greenewalt, 1960a; Weis-Fogh, 1972; Wells, 1993), but a variety of small differences in kinematics help to explain why the hovering upstroke produces less lift than the downstroke (Warrick et al., 2005). These include slightly greater values of $|\alpha|$ during early downstroke *versus* upstroke (Fig. 9), a different trajectory of the wingtips and wrists apparent in lateral projection (Fig. 2A and Fig. 7), and marginally greater angular velocity of the wing during downstroke (Fig. 5C).

Because α and α_c were measured at the middle of the wing as a line between the wrist and the tip of the first secondary, we are unable to address any potential effects of long-axis twisting of the wings (Bilo, 1971; Bilo, 1972; Willmott and Ellington, 1997a). Particularly during upstroke, the hummingbird wing twists so that the proximal and distal sections of the wing exhibit different angles relative to the body and, potentially, the incurrent air (Warrick et al., 2005). Data from other species (Bilo, 1971; Bilo, 1972; Hedrick et al., 2002) suggest that twist about the long-axis may be present during the entire wingbeat. For example, changes in α differ in magnitude and relative timing between the proximal and distal wing of the cockatiel (Hedrick et al., 2002).

New research on the patterns of wing motion in birds would, therefore, benefit from adopting a more complete protocol for measuring α_c and α along the entire wing. The strip method recommended for use in studies of insect flight may be appropriate (Willmott and Ellington, 1997a). A challenge for applying this method to birds is that cross-sectional profile and camber vary greatly along the avian wing, but laser scanning shows promise for creating useful 3D models (Liu et al., 2004). Profile, camber, α_c and α may vary throughout the wingbeat of birds (Bilo, 1971; Bilo, 1972) (Figs 4, 5 and 9). This variation is probably due aeroelasticity (Bisplinghoff et al., 1955), neuromuscular control (Dial, 1992a) and interactions between the two (Natarajan, 2002). Consequently, an effort to measure additional details of wing kinematics will remain pivotal to advancing understanding of bird flight.

Looking toward future research on flight performance in hummingbirds, caution is required when interpreting our measures of α. Two measures indicate that unsteady aerodynamic effects (Spedding, 1993; Dickinson et al., 1999) dominated during slow flight and were perhaps significant over the full range of velocity in our experiments. These effects likely make our estimate of V_i (Eqn 1–3) inaccurate, with concomitant effects on α. The measures of unsteadiness are advance ratio (J):

$$J = VT\phi b\,, \tag{4}$$

where T=wingbeat duration, and reduced frequency (k):

$$k = \pi fc / V\,, \tag{5}$$

where c=wing chord (Table 1). In our experiments, J was 0 during hovering and increased from 0.3±0.06 during flight at 2 m s^{-1} to 1.3±0.2 during flight at 12 m s^{-1}. When J=1, the forward distance traveled by the body during one wingbeat is equal to the distance traveled by the wingtip (Rosén et al., 2004). J was 0.8±0.02 during flight at 6 m s^{-1} and 1.12±0.03 during flight at 8 m s^{-1}. The expected overlap of projected paths of the wingtips with J<1 is apparent for slower velocities (0–4 m s^{-1}) in Fig. 7, indicating that the wingtips may interact with flow in the wake. For comparison, the thrush nightingale exhibits values for J decreasing from 1.2 to 0.6 over the range from 5 to 10 m s^{-1}, reaching a value of J<1 at 7 m s^{-1} (Rosén et al., 2004).

With similar consequences for the predicted likelihood of unsteady flow patterns, k in hummingbirds varied from a maximum of 0.66±0.08 during flight at 2 m s^{-1} to 0.11 during flight at 12 m s^{-1} (k is undefined for hovering, Eqn 5). Spedding (Spedding, 1993) suggests that unsteady effects are likely to be significant to the flow about the wings when k>1 and that they may be ignored when k<0.1. Hummingbirds did not achieve k<0.1 even at their fastest sustained velocity. Thrush nightingales also do not achieve this value, with a minimum k of 0.2 during flight at 10 m s^{-1} (Rosén et al., 2004). Given the complexity of the avian wingbeat, k is only a rough predictor for the likelihood of unsteady flow (Rosén et al., 2004). Nonetheless, our results reveal that the potential contribution of unsteady flow should be taken into consideration in future experiments on flight aerodynamics in hummingbirds.

List of symbols

α	angle of attack of wing
α_c	chord angle relative to mid-frontal plane of body
β	body angle relative to horizontal
γ_b	anatomical stroke-plane angle relative to mid-frontal plane of body
γ_h	tracking stroke-plane angle relative to horizontal
ρ	air density
ϕ	wingbeat amplitude
ψ_d	global downstroke-plane angle relative to horizontal
ψ_u	global upstroke-plane angle relative to horizontal
AR	aspect ratio
b	wing span
c	wing chord
CV	coefficient of variation
f	wingbeat frequency
$\boldsymbol{g}$	gravitational acceleration
k	reduced frequency
l	wing length
M_b	body mass
J	advance ratio
S_d	disc area
T	duration of wingbeat
V	free-stream velocity
V_i	induced velocity

We thank Jim Usherwood and an anonymous referee for their helpful comments on a previous draft of the manuscript. Supported by Murdock Grants 99153 and 2001208 to B.W.T. and NSF Grants IBN-0327380 and IOB-0615648 to B.W.T. and D.R.W.

References

Altshuler, D. L. and Dudley, R. (2002). The ecological and evolutionary interface of hummingbird flight physiology. *J. Exp. Biol.* **205**, 2325-2336.

Altshuler, D. L. and Dudley, R. (2003). Kinematics of hovering hummingbird flight along simulated and natural elevational gradients. *J. Exp. Biol.* **206**, 3139-3147.

Altshuler, D. L., Dudley, R. and McGuire, J. A. (2004). Resolution of a paradox: hummingbird flight at high elevation does not come without a cost. *Proc. Natl. Acad. Sci. USA* **101**, 17731-17736.

Barlow, J. B., Jr, Rae, W. H., Jr and Pope, A. (1999). *Low-Speed Wind Tunnel Testing*. New York: Wiley-Interscience.

Bartholomew, G. A. and Lighton, J. R. B. (1986). Oxygen consumption during hover-feeding in free-ranging Anna hummingbirds. *J. Exp. Biol.* **123**, 191-199.

Bilo, D. (1971). Flugbiophysik von Kleinvögeln. I. Kinematik und Aerodynamik des Flügelabschlages beim Haussperling (*Passer domesticus* L.). *Z. Vergl. Physiol.* **71**, 382-454.

Bilo, D. (1972). Flugbiophysik von Kleinvögeln. II. Kinematik und Aerodynamik des Flügelaufschlages beim Haussperling (*Passer domesticus* L.). *Z. Vergl. Physiol.* **76**, 426-437.

Bisplinghoff, R. L., Ashley, H. and Halfman, H. (1955). *Aeroelasticity*. Cambridge, MA: Addison-Wesley.

Brown, R. H. J. (1953). The flight of birds. II. Wing function in relation to flight speed. *J. Exp. Biol.* **30**, 90-103.

Brown, R. H. J. (1963). The flight of birds. *Biol. Rev.* **38**, 460-489.

Calder, W. A. (1993). Rufous Hummingbird (*Selasphorus rufus*). In *The Birds of North America.* No. 53 (ed. A. Poole and F. Gill). Philadelphia, Washington: The Academy of Natural Sciences and The American Ornithologists Union.

Chai, P. and Dudley, R. (1995). Limits to vertebrate locomotor energetics suggested by hummingbirds hovering in heliox. *Nature* **377**, 722-725.

Chai, P. and Dudley, R. (1996). Limits to flight energetics of hummingbirds hovering in hypodense and hypoxic gas mixtures. *J. Exp. Biol.* **199**, 2285-2295.

Chai, P. and Dudley, R. (1999). Maximum flight performance of hummingbirds: capacities, constraints and trade-offs. *Am. Nat.* **153**, 398-411.

Chai, P. and Millard, D. (1997). Flight and size constraints: hovering performance of large hummingbirds under maximal loading. *J. Exp. Biol.* **200**, 2757-2763.

Chai, P., Chen, J. S. C. and Dudley, R. (1997). Transient hovering performance of hummingbirds under conditions of maximal loading. *J. Exp. Biol.* **200**, 921-929.

Chai, P., Altshuler, D. L., Stephens, D. B. and Dillon, M. E. (1999). Maximal horizontal flight performance of hummingbirds: effects of body mass and molt. *Physiol. Biochem. Zool.* **72**, 145-155.

Corning, W. R. and Biewener, A. A. (1998). *In vivo* strains in pigeon flight feather shafts: implications for structural design. *J. Exp. Biol.* **201**, 3057-3065.

Dial, K. P. (1992a). Activity patterns of the wing muscles of the pigeon (*Columba livia*) during different modes of flight. *J. Exp. Zool.* **262**, 357-373.

Dial, K. P. (1992b). Avian forelimb muscles and nonsteady flight: can birds fly without using the muscles of their wings? *Auk* **109**, 874-885.

Dickinson, M. H., Lehmann, F. O. and Sane, S. P. (1999). Wing rotation and the aerodynamic basis of insect flight. *Science* **284**, 1954-1960.

Epting, R. J. (1980). Functional dependence on the power for hovering on wing disc loading in hummingbirds. *Physiol. Zool.* **53**, 347-357.

Felsenstein, J. (1985). Phylogenies and the comparative method. *Am. Nat.* **125**, 1-15.

Garland, T., Harvey, P. H. and Ives, A. R. (1992). Procedures for the analysis of comparative data using phylogenetically independent contrasts. *Syst. Biol.* **41**, 18-32.

Gatesy, S. M. and Baier, D. B. (2005). The origin of the avian flight stroke: a kinematic and kinetic perspective. *Paleobiology* **31**, 382-399.

Gill, F. B. (1985). Hummingbird flight speeds. *Auk* **102**, 97-101.

Greenewalt, C. H. (1960a). *Hummingbirds*. New York: Doubleday.

Greenewalt, C. H. (1960b). The wings of insects and birds as mechanical oscillators. *Proc. Am. Philos. Soc.* **104**, 605-611.

Hatze, H. (1988). High-precision three-dimensional photogrammetric calibration and object space reconstruction using a modified DLT-approach. *J. Biomech.* **21**, 533-538.

Hedenström, A., Griethuijsen, L. V., Rosén, M. and Spedding, G. R. (2006). Vortex wakes of birds: recent developments using digital particle image velocimetry in a wind tunnel. *Anim. Biol.* **56**, 535-549.

Hedrick, T. L., Tobalske, B. W. and Biewener, A. A. (2002). Estimates of circulation and gait change based on a three-dimensional kinematic analysis of flight in cockatiels (*Nymphicus hollandicus*) and ringed turtle-doves (*Streptopelia risoria*). *J. Exp. Biol.* **205**, 1389-1409.

Hedrick, T. L., Usherwood, J. R. and Biewener, A. A. (2004). Wing inertia and whole-body acceleration: an analysis of instantaneous aerodynamic force production in cockatiels (*Nymphicus hollandicus*) flying across a range of speeds. *J. Exp. Biol.* **207**, 1689-1702.

Liu, T., Kuykendoll, K., Rhew, R. and Jones, S. (2004). Avian wings. NASA Technical Reports Server, AIAA Paper 2004-2186, http://ntrs.nasa.gov/.

Murphy, R. C. (1913). The undulatory flight of humming-birds. *Ibis* **11**, 708-709.

Natarajan, A. (2002). Aeroelasticity of morphing wings using neural networks. PhD thesis, Virginia Polytechnic Institute and State University, USA.

Park, K. J., Rosén, M. and Hedenström, A. (2001). Flight kinematics of the barn swallow *Hirundo rustica* over a wide range of speeds in a wind tunnel. *J. Exp. Biol.* **204**, 2741-2750.

Pennycuick, C. J. (1975). Mechanics of flight. In *Avian Biology*. Vol. 5 (ed. D. S. Farner and J. R. King), pp. 1-75. New York: Academic Press.

Pennycuick, C. J., Alerstam, T. and Hedenström, A. (1997). A new low-turbulence wind tunnel for bird flight experiments at Lund University, Sweden. *J. Exp. Biol.* **200**, 1441-1449.

Rayner, J. M. V. (1985). Bounding and undulating flight in birds. *J. Theor. Biol.* **117**, 47-77.

Rayner, J. M. V. (1986). Vertebrate flapping flight mechanics and aerodynamics and the evolution of flight in bats. In *Biona Report 5, Bat Vlight – Fledermausflug* (ed. W. Nachtigall), pp. 27-74. Stuttgart: Gustav Fischer Verlag.

Rayner, J. M. V. (1988). Form and function in avian flight. *Curr. Ornithol.* **5**, 1-66.

Robinson, T. R., Sargent, R. R. and Sargent, M. B. (1996). Ruby-throated hummingbird (*Archilochus colubris*). In *The Birds of North America*. No. 204 (ed. A. Poole and F. Gill). Philadelphia, Washington: The Academy of Natural Sciences and The American Ornithologists Union.

Rosén, M. W., Spedding, G. R. and Hedenström, A. (2004). The relationship between wingbeat kinematics and vortex wake of a thrush nightingale. *J. Exp. Biol.* **207**, 4255-4268.

Sane, S. P. (2006). Induced airflow in flying insects. I. A theoretical model of the induced flow. *J. Exp. Biol.* **209**, 32-42.

Scholey, K. D. (1983). Developments in vertebrate flight: climbing and gliding of mammals and reptiles, and the flapping flight of birds. PhD thesis, University of Bristol, UK.

Sibley, C. A. and Ahlquist, J. E. (1990). *Phylogeny and Classification of Birds: A Study in Molecular Evolution.* New Haven: Yale University Press.

Spedding, G. R. (1993). On the significance of unsteady effects in the aerodynamic performance of flying animals. *Contemp. Math.* **141**, 401-409.

Spedding, G. R., Rayner, J. M. V. and Pennycuick, C. J. (1984). Momentum and energy in the wake of a pigeon (*Columba livia*) in slow flight. *J. Exp. Biol.* **111**, 81-102.

Spedding, G. R., Rosén, M. and Hedenström, A. (2003). A family of vortex wakes generated by a thrush nightingale in free flight in a wind tunnel over its entire natural range of flight speeds. *J. Exp. Biol.* **206**, 2313-2344.

Stiles, F. G. (1982). Aggressive and courtship displays of the male Anna's hummingbirds. *Condor* **84**, 208-225.

Stolpe, V. M. and Zimmer, K. (1939). Der Schwirrflug des Kolibri im Zeitlupenfilm. *J. Ornithol.* **87**, 136-155.

Tobalske, B. W. (2000). Biomechanics and physiology of gait selection in flying birds. *Physiol. Biochem. Zool.* **73**, 736-750.

Tobalske, B. W. (2001). Morphology, velocity, and intermittent flight in birds. *Am. Zool.* **41**, 177-187.

Tobalske, B. W. and Dial, K. P. (1996). Flight kinematics of black-billed magpies and pigeons over a wide range of speeds. *J. Exp. Biol.* **199**, 263-280.

Tobalske, B. W., Peacock, W. L. and Dial, K. P. (1999). Kinematics of flap-bounding flight in the zebra finch over a wide range of speeds. *J. Exp. Biol.* **202**, 1725-1739.

Tobalske, B. W., Hedrick, T. L., Dial, K. P. and Biewener, A. A. (2003a). Comparative power curves in bird flight. *Nature* **421**, 363-366.

Tobalske, B. W., Hedrick, T. L. and Biewener, A. A. (2003b). Wing kinematics of avian flight across speeds. *J. Avian Biol.* **34**, 177-184.

Tobalske, B. W., Puccinelli, L. A. and Sheridan, D. C. (2005a). Contractile activity of the pectoralis in the zebra finch according to mode and velocity of flap-bounding flight. *J. Exp. Biol.* **208**, 2895-2901.

Tobalske, B. W., Warrick, D. R. and Powers, D. R. (2005b). Effect of wing design on wake structure in small flying birds. *Integr. Comp. Biol.* **45**, 1084.

Usherwood, J. R., Hedrick, T. L. and Biewener, A. A. (2003). The aerodynamics of avian take-off from direct pressure measurements in Canada geese (*Branta canadensis*). *J. Exp. Biol.* **206**, 4051-4056.

Usherwood, J. R., Hedrick, T. L., McGowan, C. P. and Biewener, A. A. (2005). Dynamic pressure maps for wings and tails of pigeons in slow, flapping flight, and their energetic implications. *J. Exp. Biol.* **208**, 355-369.

Van den Berg, C. and Ellington, C. P. (1997). The vortex wake of a 'hovering' model hawkmoth. *Philos. Trans. R. Soc. Lond. B Biol. Sci*. **352**, 317-328.

Wakeling, J. M. and Ellington, C. P. (1997). Dragonfly flight. III. Lift and power requirements. *J. Exp. Biol.* **200**, 583-600.

Warrick, D. R. and Dial, K. P. (1998). Kinematic, aerodynamic, and anatomical mechanisms in the slow, maneuvering flight of pigeons. *J. Exp. Biol.* **201**, 655-672.

Warrick, D. R., Tobalske, B. W. and Powers, D. P. (2005). Aerodynamics of the hovering hummingbird. *Nature* **435**, 1094-1097.

Weis-Fogh, T. (1972). Energetics of hovering flight in hummingbirds and in *Drosophila*. *J. Exp. Biol.* **56**, 79-104.

Weis-Fogh, T. (1973). Quick estimates of flight fitness in hovering animals, including novel mechanisms for lift production. *J. Exp. Biol.* **59**, 169-230.

Wells, D. (1993). Muscle performance in hovering hummingbirds. *J. Exp. Biol.* **178**, 39-57.

Willmott, A. P. and Ellington, C. P. (1997a). Measuring the angle of attack of beating insect wings: robust three-dimensional reconstruction from two-dimensional images. *J. Exp. Biol.* **200**, 2693-2704.

Willmott, A. P. and Ellington, C. P. (1997b). The mechanics of flight in the hawkmoth *Manduca sexta*. II. Aerodynamic consequences of kinematic and morphological variation. *J. Exp. Biol.* **200**, 2723-2745.

Willmott, A. P., Ellington, C. P. and Thomas, A. L. R. (1997). Flow visualization and unsteady aerodynamics in the flight of the hawkmoth, *Manduca sexta Philos. Trans. R. Soc. Lond. B Biol. Sci.* **352**, 303-316.

Woltring, H. J. (1986). A FORTRAN package for generalized, cross-validatory spline smoothing and differentiation. *Adv. Eng. Software* **8**, 104-113.